European Coordination for Accelerator Research and Development

PUBLICATION

Resolution study of higher-order-mode-based beam position diagnostics using custom-built electronics in strongly coupled 3.9 GHz multi-cavity accelerating module

Zhang, P (The University of Manchester / DESY / The Cockcroft Institute) *et al*

24 May 2013

The research leading to these results has received funding from the European Commission under the FP7 Research Infrastructures project EuCARD, grant agreement no. 227579.

This work is part of EuCARD Work Package **10: SC RF technology for higher intensity proton accelerators and higher energy electron linacs**.

The electronic version of this EuCARD Publication is available via the EuCARD web site <http://cern.ch/eucard> or on the CERN Document Server at the following URL : <http://cds.cern.ch/record/1550964

Resolution study of higher-order-mode-based beam position diagnostics using custom-built electronics in strongly coupled 3.9 GHz multi-cavity accelerating module

P. Zhang[1,2,3], N. Baboi[2], R.M. Jones[1,3], N. Eddy[4]
[1]School of Physics and Astronomy, The University of Manchester, Manchester, U.K.
[2]Deutsches Elektronen-Synchrotron (DESY), Hamburg, Germany
[3]The Cockcroft Institute of Accelerator Science and Technology, Daresbury, U.K.
[4]Fermilab, Batavia, Illinois 60510, U.S.A.

Abstract

Beam-excited higher order modes (HOMs) can provide remote diagnostics information of the beam position and cavity misalignment. In this paper we report on recent studies on the resolution with specially selected series of modes with custom-built electronics. This constitutes the first report of measurements of these cavities in which we obtained a resolution of 20 micron in beam offset. Details of the setup of the electronics and HOM measurements are provided.

keywords: Beam-line instrumentation (beam position and profile monitors; beam-intensity monitors; bunch length monitors); Analysis and statistical methods; Data reduction methods

Declaration: This paper has been published by Journal of Instrumentation (ESSN: 1748-0221).

2012 JINST 7 P11016, DOI: http://dx.doi.org/10.1088/1748-0221/7/11/P11016

1 Introduction

An electron beam entering an accelerating cavity excites wakefields [1]. These wakefields may be decomposed into higher order modes (HOM). The wakefields have both longitudinal and transverse components. The short range component is related to the wakefield along the bunch. In this work we focus on the transverse component of long range wakefields, which has the potential to dilute the multi-bunch emittance [2, 3]. At FLASH [4], the amplitude of the various components of the HOMs excited by the accelerated bunch train is significantly larger in third harmonic 3.9 GHz cavities [5] than in the TESLA 1.3 GHz cavities [6]. By minimizing the power of HOMs radiated to the special couplers, the adverse effects of HOMs to the beam are mitigated. On the other hand, higher order modes contain transverse beam position information, and this enables position diagnostics inside existing third harmonic accelerating cavities without the need for additional vacuum instrumentations [7]. This is essential for aligning the beam on the electric axis of the cavities and consequently better beam quality.

Previous studies [8, 9, 10, 11] have suggested three modal options potentially suitable for position diagnostics. These are: localized dipole beam-pipe modes, coupled cavity modes in the first two dipole bands and trapped cavity modes in the fifth dipole band. We have custom designed-and-built a test electronics setup in order to study these three options with the FLASH electron beam.

This section of the paper continues with an introduction on the FLASH accelerator facility and third harmonic cavities, the fundamental of beam position diagnostics with higher order modes and the principle of the test electronics. Trapped cavity modes in the fifth dipole band provide local beam position inside the cavity, and are addressed in Section 2. A dimension reduction technique along with linear regression has been used to extract the beam position from the higher order modes. The dependence of the position resolution on various dipole modes and various time windows is studied and also explained in Section 2. The resolution when determining a four-cavity-module-based beam position is presented in Section 3 using coupled cavity modes in the second dipole band.

1.1 FLASH and the third harmonic cavities

FLASH (**F**ree-electron **LAS**er in **H**amburg) [4] is a free-electron laser facility at DESY. It uses an ultra-short electron bunch with high peak current to generate high brilliance coherent light pulses. FLASH is a user facility for photon science and a test facility for various accelerator studies. It is also a pilot facility for the European XFEL [12] and the International Linear Collider (ILC) [13].

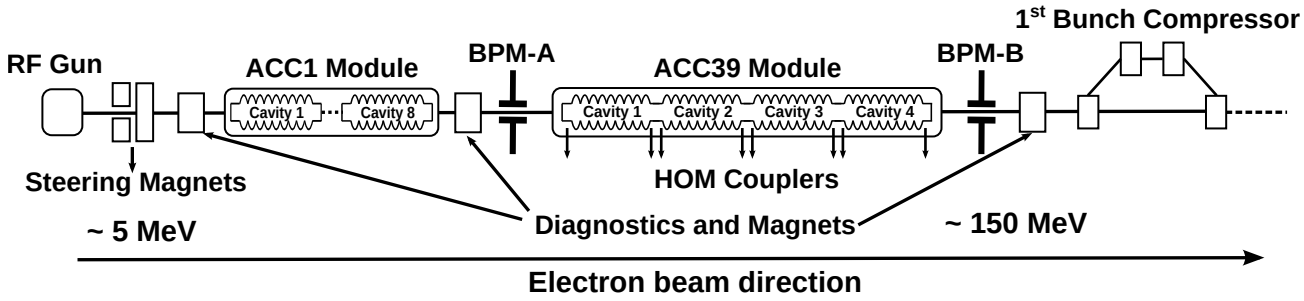

Figure 1: Schematic of injector section of the FLASH facility (not to scale, cavities in ACC1 are approximately three times larger than those in ACC39).

The injector section of FLASH is shown schematically in Fig. 1. The electron bunches of 5 MeV are produced in a laser-driven gun and accelerated to the energy of approximately 170 MeV using eight superconducting TESLA 1.3 GHz cavities contained within the subsequently ACC1 module [6]. The electron bunch is then decelerated to an energy of approximately 150 MeV using four third harmonic 3.9 GHz cavities [5]. These cavities are used to linearize the curvature of bunch's energy spread caused by the sinusoidal 1.3 GHz RF field [14]. The millimeter-long electron bunch is subsequently compressed by the first magnetic chicane to achieve a higher beam current. There are various beam instrumentations and magnets along the beam path, of which some are relevant for this study and therefore shown explicitly in Fig. 1. These are two steering magnets located upstream of the ACC1 module and two beam position monitors (BPM) on both sides of the ACC39 module.

The third harmonic 3.9 GHz cavity inherits a similar design of to the 1.3 GHz TESLA cavity. A schematic of the third harmonic cavity is illustrated in Fig. 2(a) along with important dimensions. It has one power coupler and one pick-up probe installed on the beam pipe connecting end-cells. It is also equipped with two HOM couplers installed on each side of the connecting beam pipes with different rotations as shown in Fig. 2(b) and different designs [15]. The HOM coupler located on the same side of the power coupler is named H1, while the other H2. The wakefields in the third harmonic 3.9 GHz cavity are significantly stronger than those in the TESLA 1.3 GHz cavity due to a much smaller iris radius: 15 mm compared with 35 mm [5, 6]. Unlike the TESLA 1.3 GHz cavity, most HOMs in the third harmonic 3.9 GHz cavity are above the cutoff frequencies of the connecting beam pipes in order to achieve a better damping of the HOMs [5]. However, this allows HOMs to propagate amongst cavities in the module, and thus gives rise to a dense coupled modal spectrum in the third harmonic cavity.

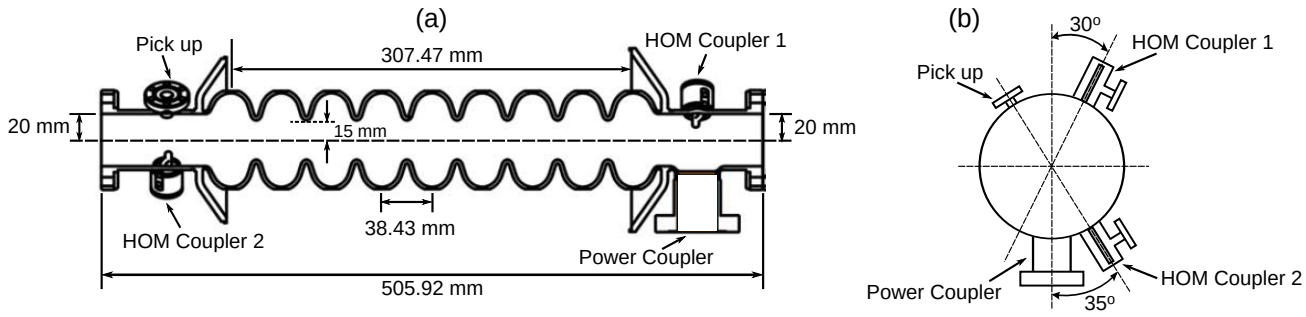

Figure 2: Schematic of a third harmonic cavity with one power coupler, one pick up probe and two HOM couplers.

1.2 Fundamentals of beam position diagnostics with HOM radiation

In order to describe the essential principle of the diagnostics, consider a simplified third harmonic cavity without couplers, which has cylindrical symmetry as shown in Fig. 3. In this structure, a particle of point charge q' is moving in the z direction with an ultra-relativistic velocity c. The particle has a transverse offset r', which is projected in Cartesian coordinates as x' and y'.

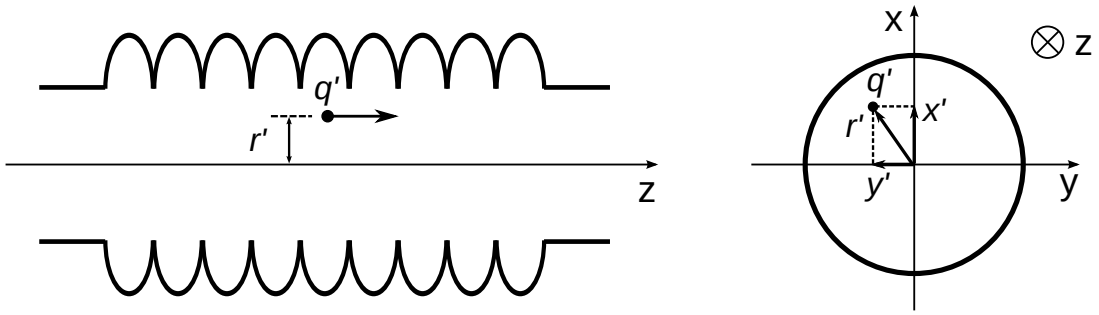

Figure 3: A point charged particle q' traversing a cavity with an offset x' and y'.

As the particle q' traverses the cavity, a wakefield is excited. This beam-excited wakefield has both longitudinal and transverse components. The former has a direct impact on the energy spread of the beam and the latter results in an emittance dilution. For diagnostics purposes we concern ourselves with the transverse wakefield. In particular we focus on the long range wakefield - i.e. the electromagnetic fields that succeeding bunches in the train experience. Close to the axis where r' is small, the transverse wake potential $\vec{W}_\perp$ is dominated by dipole modes. Performing a multi-pole expansion, $\vec{W}_\perp$ can be written as [16, 17]

$$\vec{W}_\perp \approx \left(x'\vec{e}_x + y'\vec{e}_y\right) c \sum_n^\infty \left(\frac{R}{Q}\right)_n sin\frac{\omega_n s}{c}, \quad \forall s > 0 \tag{1}$$

where $\vec{e}_x$ and $\vec{e}_y$ are unit vectors in x and y directions, $(R/Q)_n$ and ω_n are the ratio of shunt impedance to quality factor and radian frequency of the n^{th} dipole eigenmode, s is the longitudinal position behind the particle q'. From this equation, $\vec{W}_\perp$ depends linearly on the transverse position x' and y' of the particle q' inducing the wakefield. This makes it possible to determine the transverse beam position inside the cavity by examining the beam-excited dipole signal [18, 19, 20].

1.3 Principle of the test electronics

During a comprehensive series of simulations of the first six dipole bands of a third harmonic 3.9 GHz cavity [21, 22, 23], we ascertained that there are three significant regions of interest useful for beam position diagnostics. The first region contains modes which are coupled from one cavity to the next within the ACC39 module. The next region is the fifth dipole band containing trapped cavity modes. The third region is the localized dipole beam-pipe modes. Each region has its own merits. The coupled cavity region, as will be seen in Section 3, allows a superior position accuracy, whereas the trapped cavity modes or localized beam-pipe modes allow diagnostics on a localized cavity or beam pipe, but with a reduced accuracy compared to the coupled one.

A test electronics was designed to have the flexibility to study various modal options of interest as well as accommodate the large frequency bandwidths required. Its simplified block diagram is shown in Fig. 4. Each one of the four different analog bandpass filters can be connected into the chain to study localized dipole beam-pipe modes, coupled cavity modes in the first and second dipole band and trapped cavity modes in the fifth dipole band. After filtering, the signal is mixed with a selectable local oscillator (LO) to an intermediate frequency (IF) of approximately 70 MHz. The mixer is a single-side-band mixer with 26 dB image rejection. The LO frequency can be programmed in 9 MHz increments via a USB configuration and retains phase lock with the 9 MHz trigger signal by a Phase Lock Loop (PLL). This 9 MHz trigger is generated by dividing the 81.25 MHz reference signal from the FLASH master oscillator. Then the 70 MHz IF signal is further filtered with a 20 MHz analog bandpass filter to study the specific band of modes. After

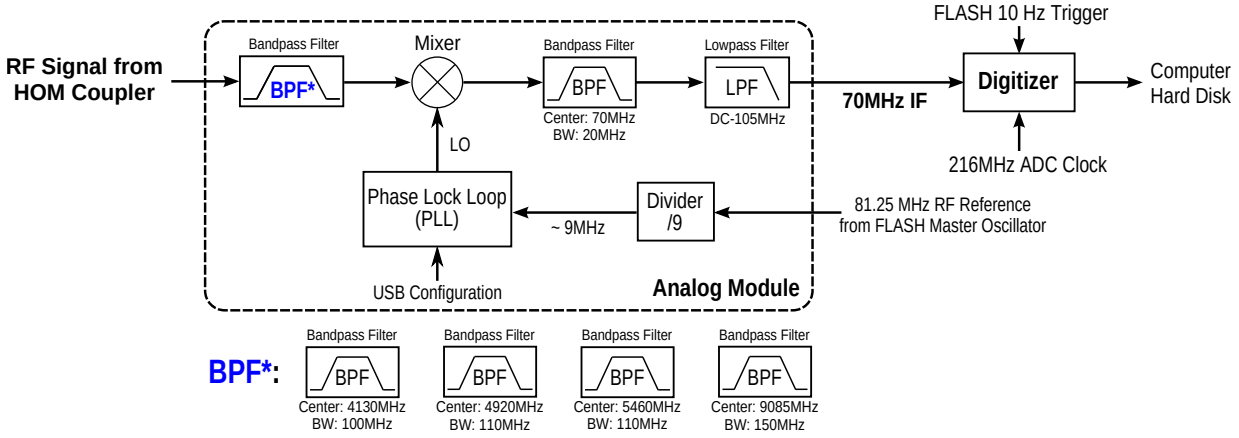

Figure 4: Schematic of the HOM electronics. Only one of the four bandpass filters was connected in front of the mixer during each measurement.

a lowpass filter, the IF signal has the frequency below 105 MHz with a dominant component from 60 MHz to 80 MHz. The signal is then digitized by a VME digitizer operating at 216 MS/s with 14 bit resolution along with a programmable FPGA for signal processing. The digitizer is triggered by a 10 Hz FLASH machine trigger. Both the selectable LO and the digitizer clock of 216 MHz are locked to the accelerator using signals delivered from the master oscillator as a reference. This locking allows correct phase information of the digitized signal. Digitized data is collected from the digitizer with the EPICS [24] software tool. The beam charge, currents of the steering magnets and BPM readouts are recorded synchronously from the FLASH control system DOOCS [25]. The data processing for position diagnostics is performed offline using MATLAB [26].

From the measurement results, coupled cavity modes in the second dipole band at approximately 5.44 GHz and trapped cavity modes in the fifth dipole band at approximately 9.06 GHz are promising for beam position diagnostics, and are described in the rest of this paper. Example waveforms of the electronics' output when connecting to HOM coupler C3H2 are shown in Fig. 5 for trapped and coupled modes. Each of them is excited by a single electron bunch. HOMs are excited at approximately 100^{th} sampling point, and then decay in a relatively short time.

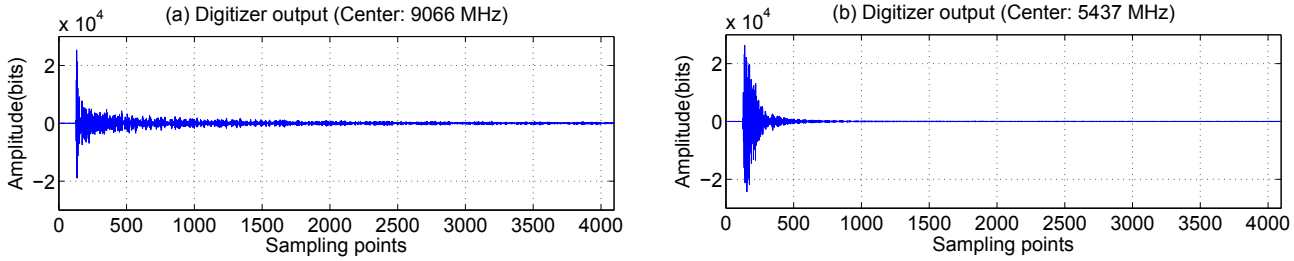

Figure 5: Signals of the digitizer output for two different bands from HOM coupler C3H2. The length of the waveform is 4096 sampling points corresponding to approximately 19 μs.

2 Position diagnostics with trapped cavity modes

In this section, data measured from HOM coupler C3H2 are described. The fourth bandpass filter in Fig. 4 was connected to obtain the fifth dipole band at approximately 9 GHz. The LO has been set to downconvert 9066 MHz to 70 MHz. An example digitizer output is shown in Fig. 5(a).

2.1 Data preparation

The frequency components of the waveform in Fig. 5(a) can be obtained by performing a FFT (Fast Fourier Transform). The magnitude of these signals are shown in Fig. 6(a). From previous studies [9, 10], we know

that modes below the double peaks at approximately 55 MHz are propagating amongst cavities, therefore an ideal filter has been applied mathematically on the waveform to cut away the frequency components below 58 MHz and above 96 MHz. Only the region within the two dash lines in Fig. 6(a) has been preserved. Since the signal decays very fast (see Fig. 5(a)), a time window has been applied on the filtered waveform to reduce the signal length. The final waveform has a length of 700 sampling points (corresponding to approximately 3.2 μs) as shown in Fig. 6(b), and will be used in the following study.

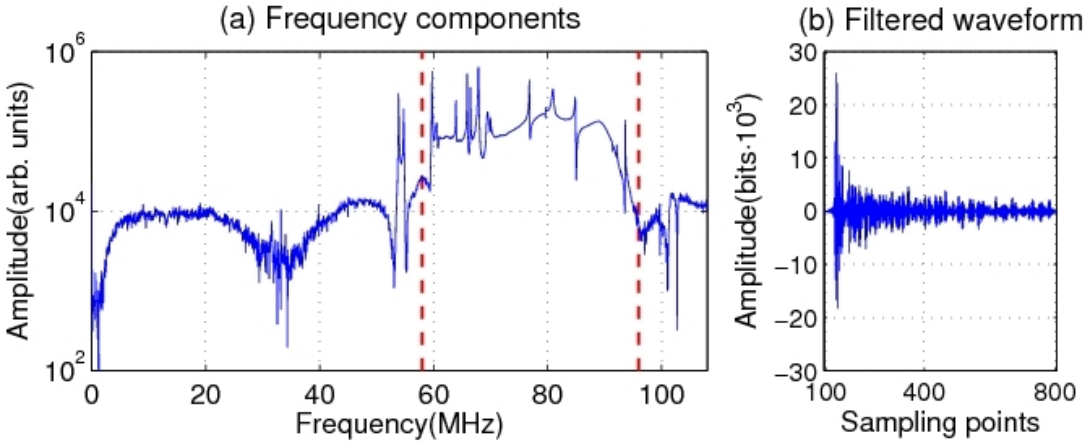

Figure 6: Frequency components of the digitized signal and a time-domain waveform after applying the ideal filter and a time window.

The beam has been moved in a 2D-grid manner by using steering magnets located upstream of the ACC1 module as shown in Fig. 1. We have switched off the non-linear elements from the RF gun up to BPM-B, i.e. the quadrupole magnets and the RF of ACC39 and removed the dark current collimator so as to create a straight-line beam trajectory. The RF of ACC1 was left on due to difficulties to transport the beam at 5 MeV. This however induces significant technical difficulties to move the beam in a random angle. Two BPMs have been used to record the transverse beam position before and after the bunch entering ACC39. These are BPM-A and BPM-B as shown in Fig. 1. The FLASH machine was operated in single bunch mode with a bunch charge of approximately 0.5 nC. A toroid situated right after BPM-B was used to record the bunch charge. A position interpolation is applied to obtain the transverse beam position in each cavity as shown in Fig. 7 for C3 as an example. These interpolated positions are used in the following study. We first took 49 calibration samples (blue dots in Fig. 7) and then 36 validation samples (red dots in Fig. 7).

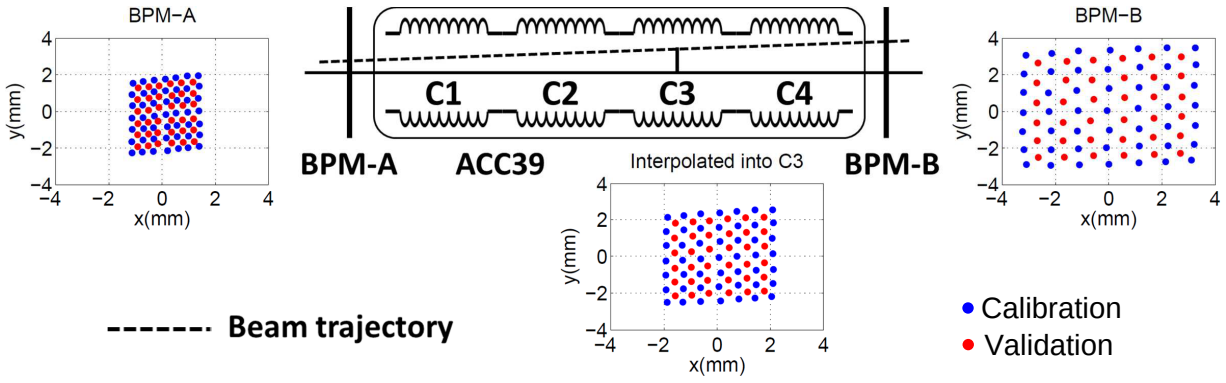

Figure 7: Position interpolated into the center of C3 from the readouts of BMP-A and BPM-B.

2.2 Extract beam position from HOM waveforms

Having the HOM waveforms and the interpolated beam positions, a linear regression is used to determine their correlations. Prior to the linear regression, a singular value decomposition (SVD) [27] method is applied on the HOM waveforms. This is used to reduce the dimension of the linear system and suppress noises present

in the HOM waveforms. The singular value of each SVD mode decomposed from the calibration samples (blue dots in Fig. 7) is shown in Fig. 8(a). The first several SVD modes have relatively large singular values, therefore their SVD mode amplitudes are used to regress on the interpolated beam positions instead of the original HOM waveforms. A calibration of the HOM signals is generated in this manner. The predictions of beam position are made by applying the calibration on the validation samples. These predictions are then compared with the measured position interpolated into the cavity. The rms of the position residuals (rms error) is defined as the position resolution.

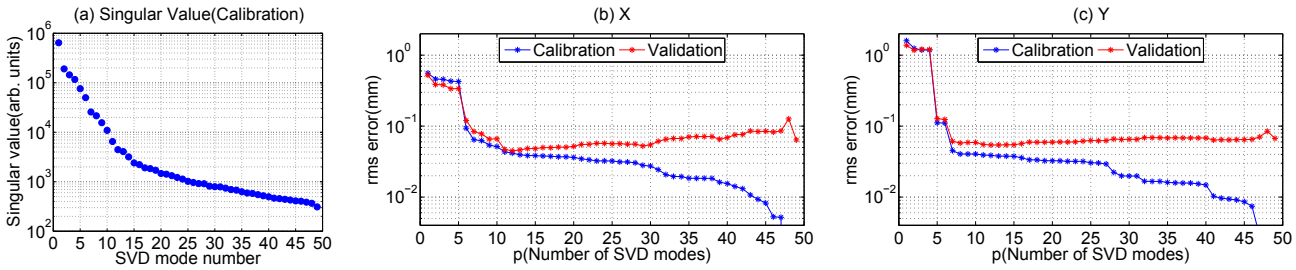

Figure 8: (a) Singular value of each SVD mode from calibration samples. (b)(c) Contribution of the first p SVD modes to determine the transverse beam position x and y measured by the rms error.

The contribution of using the first p SVD modes to determine the beam position is shown in Fig. 8(b) for x and Fig 8(c) for y. The first twelve SVD modes provide a surprisingly small rms error in both x and y for our purposes.

Focusing on analysis using the first twelve SVD modes, predictions of beam position are obtained and compared with the measured beam position as shown in Fig. 9(a). A coefficient of determination r^2 [28] is calculated to characterize the overall prediction errors. The residuals are shown in Fig. 9(b) and Fig. 9(c). From this we ascertain a position resolution of 45 μm for x and 54 μm for y.

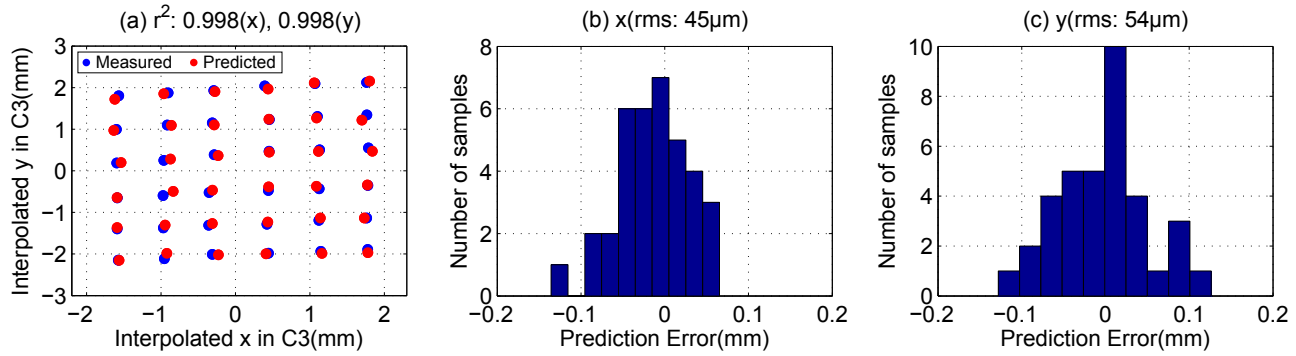

Figure 9: Prediction of the transverse beam position using the first twelve SVD modes. (a) Measurement is in blue and prediction is in red. Points connected with black lines belong to the same beam position. (b)(c) Prediction errors of x and y. The position resolution is denoted as the rms value.

2.3 The search for suitable dipole modes

Detailed simulations [21, 22, 23] have shown that modes in the fifth dipole band have small R/Q's, and therefore couple weakly to the beam. This will affect the resolution of beam position in the cavity measured with these dipole modes. In order to improve the resolution, we use a band of modes for position determination as shown in the previous section. This is different from the previous study in [20], which uses two polarizations of one dipole mode. In Fig. 10(a), the resolutions for x and y using a band of modes are shown as the long magenta lines on the bottom. These are compared with resolutions using different segments of the band. The color of the segment in Fig. 10(b) matches the color of the resolution lines in Fig. 10(a). An ideal filter is applied mathematically on the time-domain digitizer output (Fig. 5(a)) using the bandwidth of each segment in Fig. 10(b). A time window is then applied on the filtered waveform to truncate the signal

properly. Fig. 10(a) reveals a remarkable improvement in the resolution achieved through combining modes in the trapped band.

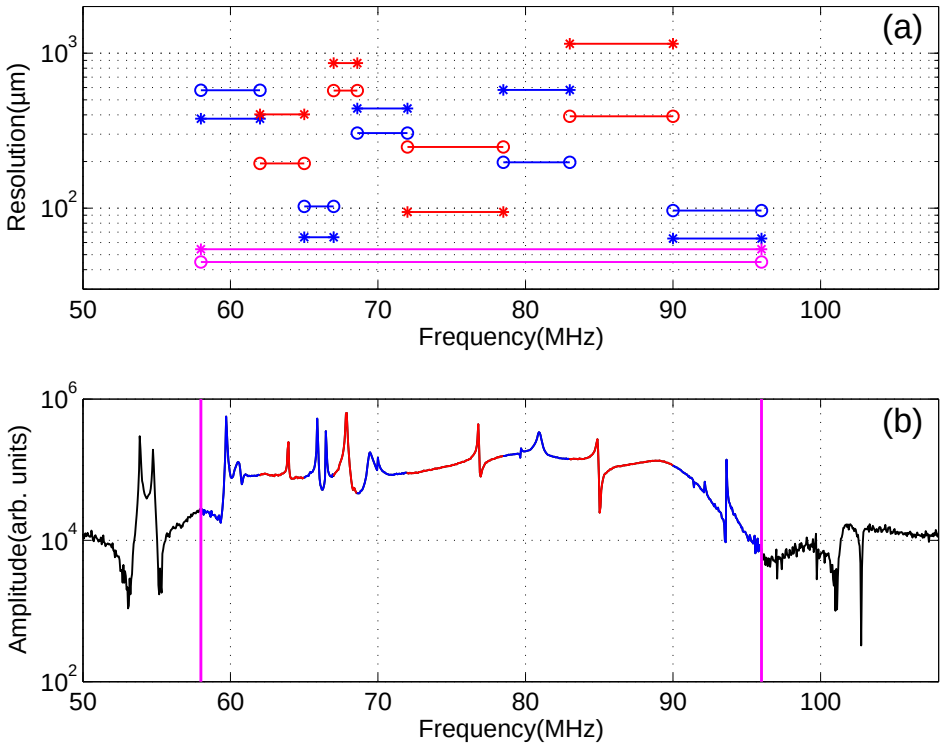

Figure 10: Resolutions of each segment of spectrum. Circles denote x and asterisks denote y.

Due to a smaller size of the third harmonic 3.9 GHz cavity compared to the TESLA 1.3 GHz cavity, the eigenmodes of ACC39 are particularly sensitive to small geometrical errors. Predicting the exact frequency locations of these modes is impractical. This is another reason to utilize the signal of a complete band of frequencies to accommodate the frequency shifts of dipole modes extracted from different cavities.

2.4 The search for a suitable time window

HOMs in the fifth dipole band decay rapidly as shown in Fig. 5(a). In this section, we study the resolution dependence on the time window applied on the waveforms. Starting from the 100^{th} sampling point, the length of the time window increases in the forward direction by a step of 50 sampling points. This is illustrated in Fig. 11(a). The waveforms with each time window are then treated with SVD and various number of SVD modes are subsequently used for position determination. The resolutions are shown in Fig. 11(b) and Fig. 11(c) for different time window and different number of SVD modes. In Fig. 11(b), a minimum length of time window starting from the 100^{th} and ending at the 300^{th} sampling point with eleven SVD modes gives a reasonably good resolution of 47 μm for x. The same time window with nine SVD modes suggest a resolution of 49 μm for y as shown in Fig. 11(c).

Having found the smallest end index, the 300^{th}, of the time window from the forward scan, we conduct a backward scan by moving the start index of the sampling point in the backward direction with a step of 10 sampling points. This is shown in Fig. 12(a). A shorter time window from the 140^{th} to the 300^{th} with eleven SVD modes give a same resolution of 47 μm for x as shown in Fig. 12(b). A resolution of 51 μm for y is expected by using the same time window with nine SVD modes as shown in Fig. 12(c).

The findings from the forward and backward scans are summarized in Table 1. The length of the time window is also calculated in terms of time. As a comparison, the resolutions with the time window used in the previous section are also listed. In an extreme case, the full length of the waveforms is also treated in the same way and resolutions are calculated. From the table, we conclude that a small length of waveform contains enough information to determine beam position with reasonably good resolution. The first 40 sampling points (from the 100^{th} to 140^{th}, corresponding to approximately 0.19 μs) which have large amplitude appear to be insensitive to beam movement. This might be due to a beam pulse effect.

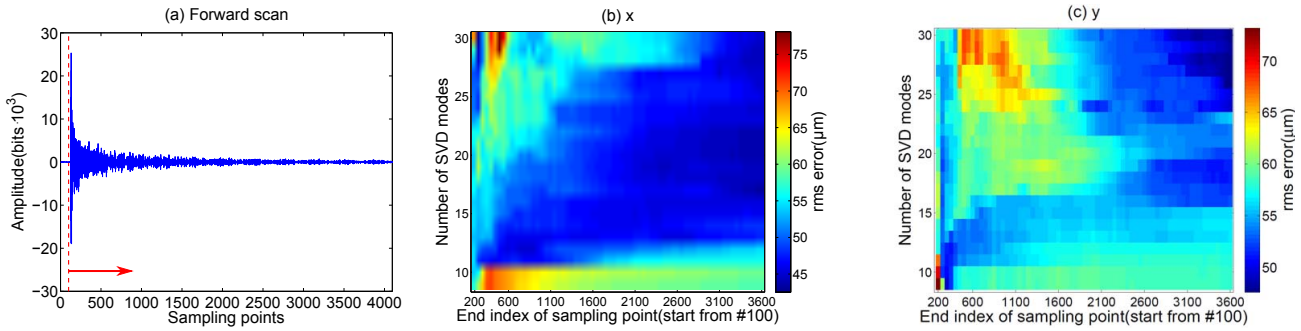

Figure 11: Scan forward starting from the 100^{th} sampling point.

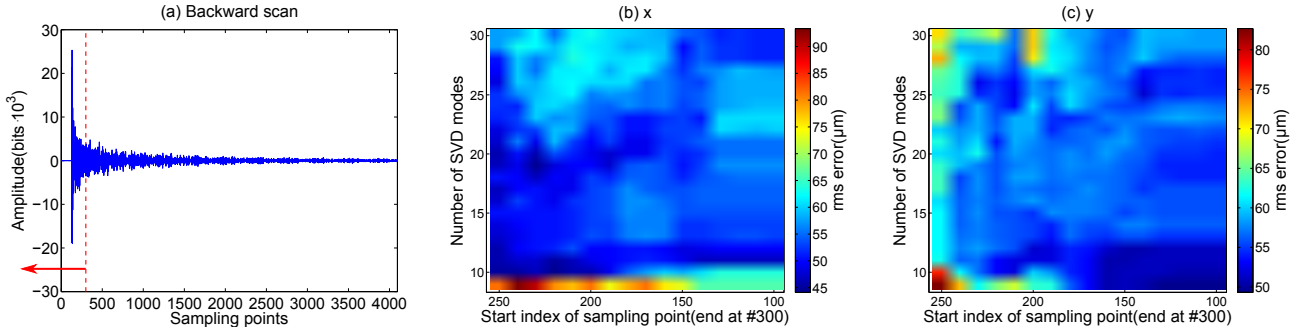

Figure 12: Scan backward ending at the 300^{th} sampling point.

As shown in Table 1, the backward scan suggests a time window from 140^{th} to 300^{th} with a length of 0.7 μs. This length is shorter than the bunch separation of 1 μs at FLASH when operated in a multi-bunch mode [4]. Fig. 13 shows the waveform with different time windows. The black lines represent the multiple bunches separated by 1 μs, while the red dash lines define the shortest time window found with reasonably good position resolution. This suggests non-degenerate position resolutions of the leading bunch in a bunch train. Although HOMs seem to decay fast, there is still a remaining signal from the current bunch overlapping with HOMs excited by the trailing bunches. This will dilute the beam position resolution of bunches following the leading bunch in a train at FLASH. However, degenerate beam positions of trailing bunches are also useful.

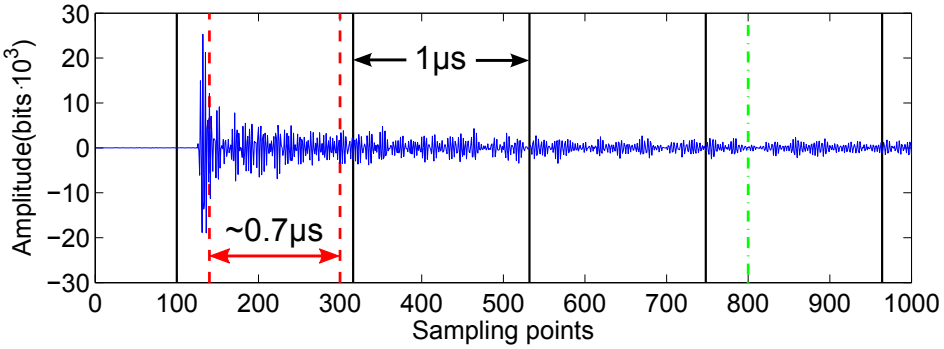

Figure 13: Waveform with various time window.

Table 1: Resolution of various segments of waveform with different number of sampling points.

	Sampling points			Resolution		SVD modes	
	start index	end index	time (μs)	x (μm)	y (μm)	x	y
Forward scan	100	300	0.9	47	49	1^{st}–11^{th}	1^{st}–9^{th}
Backward scan	140	300	0.7	47	51	1^{st}–11^{th}	1^{st}–9^{th}
Full segment	100	800	3.2	45	54	1^{st}–12^{th}	1^{st}–12^{th}
Full waveform	1	4096	18.9	43	45	1^{st}–17^{th}	1^{st}–25^{th}

3 Position diagnostics based on a band of coupled cavity modes

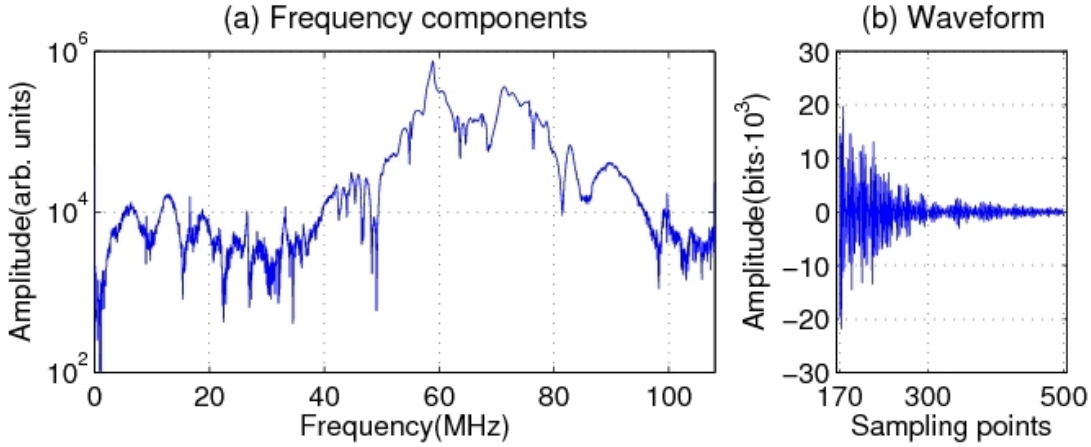

Figure 14: Frequency components of the digitized signal and a waveform slice after applying a time window.

Previous studies [8, 10] have shown that modes in the first two dipole bands propagate amongst all cavities within the ACC39 module. This enables the beam position to be determined in a four-cavity-module sense rather than an individual cavity. Therefore, we interpolate the two BPM readouts into the center of the module and study the beam position resolutions at this location. Simulations predict some strong coupling modes (with large R/Q values) in the first two dipole bands [21, 22, 23]. HOM BPMs using these modes will potentially have higher resolutions. In this section, modes in the second dipole band measured from HOM coupler C3H2 are used. The third bandpass filter in Fig. 4 was connected. The LO has been set to downconvert 5437 MHz to 70 MHz. An example digitizer output is shown in Fig. 5(b). The frequency components obtained by a FFT are shown in Fig. 14(a). A time window has been applied to cut away the saturated part of the waveform at the beginning of the signal (cut at the 170^{th} sampling point), as well as the trailing part due to a fast signal decay (end at the 500^{th} sampling point). The resulting waveform is shown in Fig. 14(b). These waveform slices are used to determine the beam position at the center of the module.

Using the first eleven SVD modes, the predicted positions are compared with measured ones as shown in Fig. 15(a). Excellent consistency can be observed. The position resolution is 20 μm for x and 23 μm for y as shown in Fig. 15(b) and Fig. 15(c).

To study the electromagnetic energy distribution of these coupled modes, the HOM power is integrated over a frequency range from 1 MHz to 107 MHz (see Fig. 14(a)) for each beam position. The power distribution of these coupled modes extracted from each HOM coupler is shown in Fig. 16. A similar position with minimum power can be found from all eight couplers although the exact distribution for each coupler is dissimilar. This might be due to different orientations of the couplers as shown in Fig. 2(b) and different types [15], therefore individual coupling to the HOMs. The longitudinal electromagnetic field distribution of these coupled modes can also contribute. Around this common position with minimum HOM power, a smaller scan was conducted as shown in Fig. 17(a). The resolution of predicting the transverse beam position at the center of the four-cavity module is obtained by using the HOM signal extracted from each of the eight couplers. This is shown in Fig. 17(b). Our study predicts a resolution of 10–25 μm for x and 20–30 μm for y.

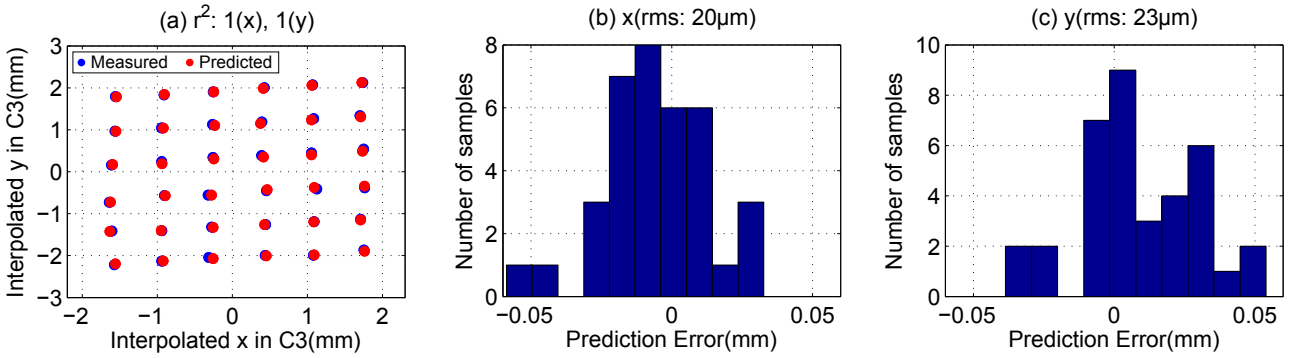

Figure 15: Prediction of the transverse beam position using the first eleven SVD modes. (a) Measurement is in blue and prediction is in red. Points connected with black lines belong to the same beam position. (b)(c) Prediction errors of x and y. The position resolution is denoted as the rms value.

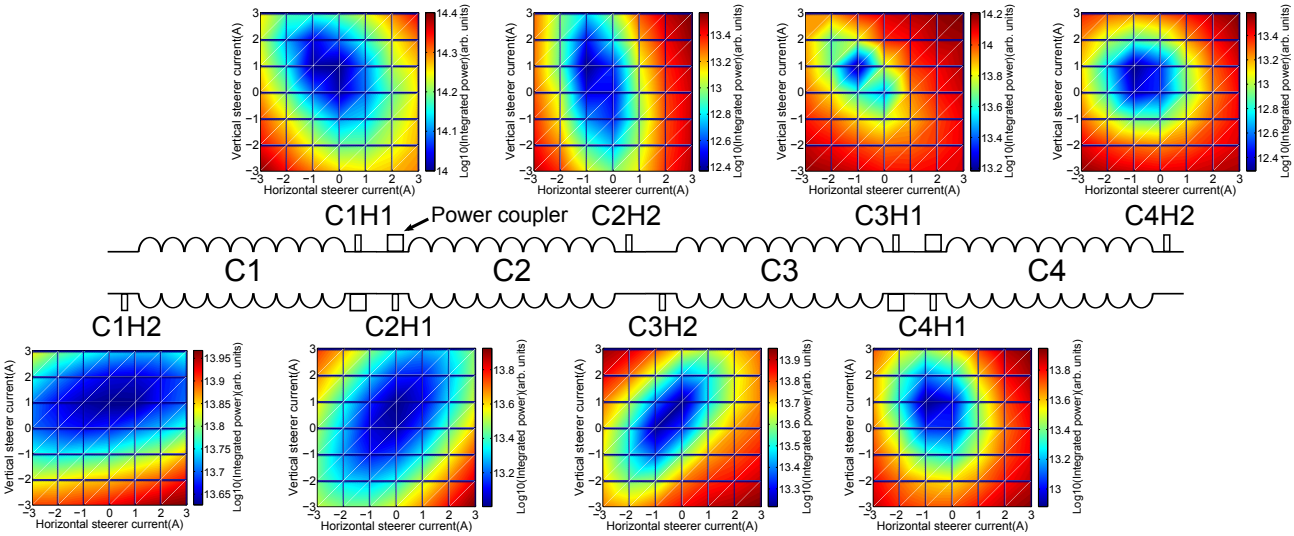

Figure 16: Integrated power (log scale) as a function of steering magnets' current.

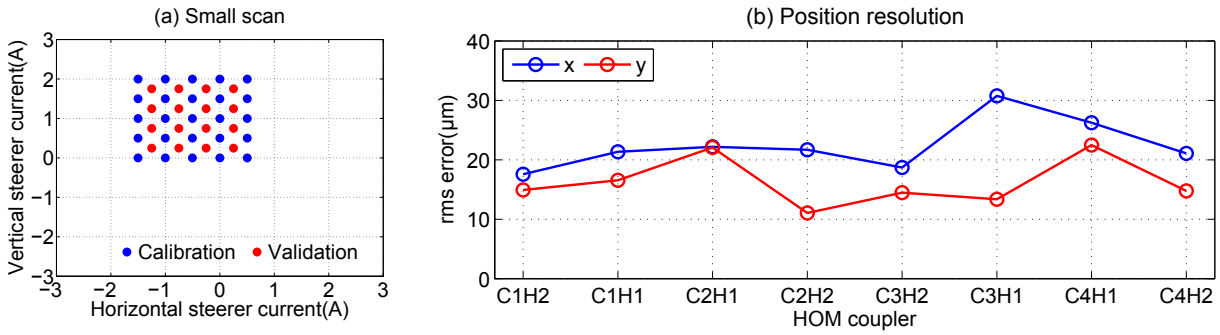

Figure 17: Small scan (a) and the corresponding position resolution for each coupler (b).

4 Final remarks

The modes within the ACC39 third harmonic accelerating module fall into two distinct categories: trapped modes and coupled inter-cavity modes. A detailed study based on experiments at the FLASH facility has been conducted in order to assess their relative merits and potential resolution. We have studied various modal options with a test electronics. Based on the measurement results, one band for each category appears to be promising for beam position diagnostics. The trapped cavity modes are used to determine the individual beam position in each cavity, and the resolution is approximately 50 μm. The transverse beam position at the center of the accelerating module can be determined by using the coupled modes, and the resolution is approximately 20 μm due to the strong coupling of these modes to the beam. A set of dedicated electronics is being built using modes in the second dipole band and the fifth dipole band, in order to facilitate high resolution measurements for the whole module, and reasonable resolution for localized measurements within individual cavities. Based on the results of this study, we anticipate providing similar HOM diagnostics for the European XFEL third harmonic module consisting of eight cavities.

Acknowledgments

Many people have contributed to the success of this work. In particular we acknowledge the invaluable contributions to the development of the test electronics and measurements from DESY scientists: Bastian Lorbeer and Thomas Wamsat, and Fermilab scientists: Brian Fellenz and Manfred Wendt. This work received support from the European Commission under the FP7 Research Infrastructures grant agreement No.227579.

References

[1] A.W. Chao and M. Tigner, *Handbook of Accelerator Physics and Engineering*, ch. 3.2, p. 196. World Scientific, first ed., 1999.

[2] R.M. Jones, "Wake field Suppression in High Gradient Linacs for Lepton Linear Colliders," *Phys. Rev. ST Accel. Beams*, vol. 12, p. 104801, 2009.

[3] J.S. Sekutowicz, "HOM Damping and Power Extraction from Superconducting Cavities," in *Proceedings of LINAC 2006*, (Knoxville, Tennessee, USA), pp. 506–510, 2006.

[4] W. Ackermann *et al.*, "Operation of a free-electron laser from the extreme ultraviolet to the water window," *Nature Photonics*, vol. 1, pp. 336–342, 2007.

[5] J. Sekutowicz, R. Wanzenberg, W.F.O. Mueller and T. Weiland, "A Design of a 3rd Harmonic Cavity for the TTF 2 Photoinjector," TESLA-FEL Report: TESLA-FEL 2002-05, 2002.

[6] J. Sekutowicz, *Multi-cell Superconducting Structures for High Energy e+e- Colliders and Free Electron Laser Linacs*. Warsaw, Poland: Warsaw University of Technology Publishing House, first ed., 2008.

[7] N. Baboi *et al.*, "Higher Order Modes for Beam Diagnostics in Third Harmonic 3.9 GHz Accelerating Modules," in *Proceedings of SRF2011*, (Chicago, USA), pp. 239–243, 2011.

[8] P. Zhang *et al.*, "Beam-based HOM Study in Third Harmonic SC Cavities for Beam Alignment at FLASH," in *Proceedings of DIPAC2011*, (Hamburg, Germany), pp. 77–79, 2011.

[9] P. Zhang, N. Baboi, R.M. Jones and I.R.R. Shinton, "Study of Beam Diagnostics with Trapped Modes in Third Harmonic Superconducting Cavities at FLASH," in *Proceedings of IPAC2011*, (San Sebastian, Spain), pp. 2891–2893, 2011.

[10] P. Zhang, N. Baboi and R.M. Jones, "Higher order mode spectra and the dependence of localized dipole modes on the transverse beam position in third harmonic superconducting cavities at FLASH," DESY Report: DESY 12-109, 2012.

[11] P. Zhang, N. Baboi, R.M. Jones, I.R.R. Shinton, T. Flisgen and H.W. Glock, "A study of beam position diagnostics using beam-excited dipole modes in third harmonic superconducting accelerating cavities at a free-electron laser," *Rev. Sci. Instrum.*, vol. 83, p. 085117, 2012.

[12] "The European X-Ray Free-Electron Laser," Technical design report: DESY 2006-097, 2007.

[13] "International Linear Collider: A Technical Progress Report," Interim Report, 2011.

[14] K. Flottmann, T. Limberg and Ph. Piot, "Generation of Ultrashort Electron Bunches by Cancellation of Nonlinear Distortions in the Longitudinal Phase Space," TESLA-FEL Report: TESLA-FEL 2001-06, 2001.

[15] T.N. Khabiboulline, I.G. Gonin and N. Solyak, "New HOM Coupler Design for 3.9 GHz Superconducting Cavities at FNAL," in *Proceedings of PAC07*, (Albuquerque, New Mexico, USA), pp. 2259–2261, 2007.

[16] K.L.F. Bane, "Wake Field Effects in a Linear Collider," SLAC Note: SLAC-PUB-4169, 1986.

[17] R. Wanzenberg, "Monopole, Dipole and Quadrupole Passbands of the TESLA 9-cell Cavity," TESLA Report: TESLA 2001-33, 2001.

[18] G. Devanz, M. Jablonka, C. Magne, O. Napoly, M. Huening and M. Wendt, "HOM Beam Coupling Measurements at the TESLA Test Facility (TTF)," in *Proceedings of EPAC2002*, (Paris, France), pp. 230–232, 2002.

[19] N. Baboi, G. Kreps, M. Wendt, G. Devanz, R. Paparella and O. Napoly, "Preliminary Study on HOM-Based Beam Alignment in the TESLA Test Facility," in *Proceedings of LINAC 2004*, (Lübeck, France), pp. 117–119, 2004.

[20] S. Molloy *et al.*, "High precision superconducting cavity diagnostics with higher order mode measurements," *Phys. Rev. ST Accel. Beams*, vol. 9, p. 112801, 2006.

[21] T. Khabibouline, N. Solyak and R. Wanzenberg, "Higher Order Modes of a 3rd Harmonic Cavity with an Increased End-cup Iris," TESLA-FEL Report: TESLA-FEL 2003-01, 2003.

[22] I.R.R. Shinton and N. Juntong, "Compendium of Eigenmodes in Third Harmonic Cavities for FLASH and the XFEL," DESY Report: DESY 12-053, 2012.

[23] P. Zhang, N. Baboi and R.M. Jones, "Eigenmode simulations of third harmonic superconducting accelerating cavities for FLASH and the European XFEL," DESY Report: DESY 12-101, 2012.

[24] EPICS. http://www.aps.anl.gov/epics/.

[25] DOOCS. http://tesla.desy.de/doocs/.

[26] MATLAB®. Ver. R2011b, The MathWorks Inc., USA, http://www.mathworks.com/.

[27] G.H. Golub and C.F. Van Loan, *Matrix Computations*, ch. 2.3, pp. 16–20. The John Hopkins University Press, second ed., 1984.

[28] R.L. Ott and M. Longnecker, *An Introduction to Statistical Methods and Data Analysis*, ch. 11.7, p. 611. Duxbury Press, sixth ed., 2008.